Analyzing Pulsar Timing Array Data through the Factorized Likelihood Approach

Levi Schult, Stephen Taylor, Scott Ransom

This thesis is submitted in partial completion of the requirements of the BS Astronomy-Physics Major.

Astronomy Department

University of Virginia

Charlottesville, VA. USA

May 15th, 2021

Abstract

Pulsar Timing Arrays (PTA) utilize the extreme temporal precision of pulsars to search for the evidence of Gravitational Waves (GWs) hidden in their timing residuals. This thesis traces the recent history and results of contemporary PTAs, pulsar timing, and the statistical methods utilized in analyzing them. The Factorized Likelihood approach is described and explored using experiments to synthesize data combinations between PTA experiments, cross-validation techniques, and Dropout analyses to determine the robustness of a GW signal in a PTA.

Contents

Chapter 1

Introduction

Pulsar Timing Arrays (PTAs, Detweiler [1979] Foster and Backer [1990]) are the next frontier in gravitational wave physics and will reveal new information about Super Massive Black Hole Binaries (SMBHB) in the universe. PTAs utilize a web of millisecond pulsars to create a galaxy-sized Gravitational Wave (GW) detector tuned to low-frequency signals [Bailes et al., 2021]. Pulsar timing is the method that makes this possible as each pulsar in the array is precisely studied such that any deviations from the model point toward unmitigated signals such as those from GWs. To determine whether or not these deviations, or Time of Arrival (TOA) residuals, are the result of gravitational waves, the many noise processes present in pulsar timing data must be well understood. GW signals will initially be detectable as a common red noise process seen in all the pulsars in the array, but this is not definitive proof (Rosado et al. [2015], Romano et al. [2021]). Definitive proof will come in the unique spatial correlation pattern between pulsars which is known as the Hellings-Downs correlation [Hellings and Downs, 1983].

PTAs are sensitive to the low-frequency regime of GWs which have not been directly detected yet. Currently, only the high-frequency regime of GWs has been observed by the ground-based interferometer experiments of the Laser Interferometer Gravitational-Wave Observatory (LIGO) and Virgo collaboration [Abbott et al., 2016]. The sources of these GWs vary depending on the frequency observed. For the high-frequency waves studied by ground-based interferometers, the sources are cataclysmic merger events between black holes, neutron stars, and other compact objects. Space-based interferometers like the Laser

Interferometer Space Antenna (LISA) will probe the mid-frequency range of GWs, studying intermediate mass black holes, extreme-mass ratio inspirals, and the merger of some high mass black hole systems. The low-frequency regime explored by PTAs will consist of gravitational waves generated by cosmic strings and the ensemble of SMBHBs in the process of merging (Bailes et al. [2021], Amaro-Seoane et al. [2017]). A stochastic background of these GWs consisting of the ensemble of the different sources is expected to be detected before individual sources [Rosado et al., 2015]. Investigating this stochastic GW background will reveal new information about the history of galaxy collisions and evolution in the universe. Hidden in this background are also strong-field tests of General Relativity. Once this background is characterized, individual sources could be resolved allowing for simultaneous study of black hole binaries using GWs and electromagnetic observations. This multi-messenger study of SMBHBs would reveal new information about these critical pieces of galactic dynamics [Lommen, 2015].

There are several PTA experiments around the world, the largest of which is the International Pulsar Timing Array (IPTA). The IPTA combines the efforts of the NANOGrav, Parkes (PPTA), European (EPTA), and now Indian (InPTA) PTA experiments to create an even more sensitive GW detector. Siemens et al. [2013] state that in the weak-signal regime (i. e. the present era without a significant detection yet) the sensitivity to a stochastic GW background will scale as T^{β} where T is the baseline of the array and β is the spectral index of the background. Further, they find that eventually the signal to noise ratio of the background scales as $\sqrt{T}$ and the addition of pulsars to the array is more important to improve the array's sensitivity. These PTA experiments release datasets on a roughly biennial basis of pulsar timing solutions and pulse Times of Arrival (TOA) which can be analyzed for evidence of GWs. The NANOGrav nine-year dataset, EPTA data release 1, and the PPTA data release 1 extended were combined into the IPTA Data Release 2 (IPTADR2) [Perera et al., 2019]. Although these constituent datasets have been used in GW searches and are well understood, their combined product has not. Our work this year served to probe the dataset for GW signals, test new, faster analysis methods, and improve existing methods.

The NANOGrav nine-year dataset consists of observations of 37 pulsars over the 2004 to 2013 period. These observations were made using the Green Bank Telescope (GBT) and

the William E. Gordon Telescope of Arecibo Observatory. Only two pulsars were observed with both telescopes: PSRs J1713+0747 and B1937+21. All other pulsars were observed as dictated by the declination range of the Arecibo telescope, which could observe declinations $0° < \delta < 39°$. The pulsars were observed with monthly cadences with some deviations due to telescope availability. Common with pulsar timing observations, each pulsar was observed at two different frequencies to account for frequency-dependent dispersion. For analysis, only pulsars with timing baselines greater than three years were used. Bayesian techniques were utilized in a modified way, where individual pulsar noise studies were performed to determine white noise parameters which were then fixed for low-frequency process searches. Analysis of the NANOGrav nine-year dataset revealed an upper limit for the dimensionless strain amplitude of $A_{GW} = 1.5 \times 10^{-15}$ at a characteristic frequency of 1/year when the GW background is modeled as a power law resulting from SMBHBs [Arzoumanian et al., 2016].

The NANOGrav 11-year dataset improves upon the nine-year dataset by adding eight pulsars to the array and two additional years of timing data. Additionally there was a campaign to observe six pulsars weekly to increase the array's sensitivity to individual sources of GWs [Burt et al., 2011] [Simon et al., 2014]. The study of this dataset introduced several advances in the search for GWs in PTA. New software such as BAYESEPHEM [Vallisneri et al., 2020], to incorporate the uncertainties in the Solar System Barycenter (SSB) in its Bayesian frameworks, and Enterprise [Ellis et al., 2019], to carry out these Bayesian studies, lay the foundation for future analyses. The development of BAYESEPHEM was critical as these SSB uncertainties can introduce noise into the PTA if ignored or left unmitigated. A novel technique was also utilized, which was first used in Aggarwal et al. [2019], that measured the level of support for the common process signal within each pulsar. This technique, dubbed the Dropout analysis, was a part of the MCMC wherein the dropout parameter for each pulsar was determined, illuminating the degree of support for the GW signal. Bayesian frameworks to search for GW signals within the data followed the precedence set by the NANOGrav nine-year dataset. At the dataset's most sensitive frequency, 8nHz, the sky-averaged strain upper limit was $h_0 < 7.3(3) \times 10^{-15}$ [Aggarwal et al., 2019].

The NANOGrav 12.5 year dataset continued to broaden the horizons of its predecessor, with 2 more pulsars and 1.5 years of timing data added to the 11-year dataset. Further,

it used 45 pulsars with timing baselines greater than three years in its GW searches. This dataset also implemented new steps to improve consistency across pulsars and the pulse profiles used to generate TOAs. In analyzing the dataset, a variety of models were used to probe the complexities of strong evidence, $\log_{10}$ Bayes factor of 4.5 when using the solar system ephemeris model DE438, in favor of a common-spectrum process with $\gamma = 13/3$ which is the spectral index for a GW background generated by SMBHBs with circular orbits. They further found inconclusive evidence for quadrupolar spatial correlations of the Hellings-Downs form, known as the definitive evidence of GWs rather than another low-frequency process. These investigations also found that monopolar and dipolar spatial correlations such as those from clock errors or solar system ephemeris uncertainties were disfavored by the Bayesian posteriors. An important additional method for quantifying the detected common process was that of the Factorized Likelihood, a key tool in the analyses presented in this paper. This Factorized Likelihood was also used to calculate dropout factors to determine each pulsar's evidence for the common process seen by the array. The descriptions of these methods are given in Section 2 [Arzoumanian et al., 2020].

The EPTA first data release is composed of 42 pulsars with baselines ranging from 6 to 24 years, ending with observations from mid-2014. A collection of telescopes across Europe were used to observe these pulsars, including the Effelsberg radio telescope, the Lovell radio telescope, the Nançay radio telescope, and the Westerbork Synthesis radio telescope. At the Effelsberg radio telescope, pulsars were observed on a roughly monthly basis at frequencies of 1410 MHz or 1360 MHz and 2639 MHz. Pulsars observed at the Lovell radio telescope had a cadence of 10 days at frequencies of 1400 MHz or 1520 MHz after a significant backend upgrade. The Nançay radio telescope recorded data at a central frequency of 1.4 or 1.6 GHz beginning in 2004, and the Westerbork Synthesis telescope observed pulsars monthly at 350 MHz, 840 MHz, and 1380 MHz [Desvignes et al., 2016]. Analysis of this dataset using five pulsars which provide the most sensitivity in the array revealed an upper limit on the GW background formed by SMBHBs of 6×10^{-15} [Lentati et al., 2015].

Manchester et al. [2013] detail the PPTA's extended first data release which contains observations of 20 pulsars spanning 17.1 years. These observations were made with the Parkes 64 meter radio telescope at 700, 1400, and 3100 MHz with a cadence of approximately

to to three weeks. This dataset was updated in Reardon et al. [2016] where legacy data was added and improved noise modeling was implemented. An analysis of this dataset revealed a an upper limit to the GW background amplitude at a one year characteristic frequency to be 1.0×10^{-15} (Manchester et al. [2013], Shannon et al. [2013], & Shannon et al. [2015]).

These datasets were combined into IPTADR2 by Perera et al. [2019]. Additionally legacy data was included for NANOGrav and the PPTA. NANOGrav's legacy data included that of PSR J1713+0747 from Zhu et al. [2015] and PSRs J1857+0943 and J1939+2134 from Kaspi et al. [1994]. The legacy data included for the PPTA was that which was included in Reardon et al. [2016]. Additional data used for GW analysis in Shannon et al. [2015] was also included in the PPTA addition to IPTADR2. Bringing these datasets together creates an array of 65 pulsars with increased sky coverage when compared to IPTADR1. To combine these datasets Perera et al. [2019] aggregated the TOAs for each pulsar across the three PTAs and then fit the timing model to the new combined set of TOAs using the TEMPO2 timing package (Hobbs et al. [2006], Hobbs et al. [2009], & Edwards et al. [2006]). Timing offsets to mitigate systematic delays between observatories were put in place as well, using the dataset with the largest sum of $1/\sigma^2$, where σ is the TOA uncertainty, as the reference dataset. The measured topocentric TOAs are converted to Solar-System Barycentric Coordinate Time (TCB) using ephemeris DE436 using the Terrestrial Time standard BIPM2015.

The standard Bayesian methodology for determining the evidence for GWs within PTA data is extremely computationally expensive. Even as early as the NANOGrav nine-year dataset, a full Bayesian search where all white, red, and GW noise parameters are allowed to vary was not possible. This is due to the large parameter spaces, encompassing six or more noise parameters for each pulsar in the array (assuming power law red noise and GW background). The PTA likelihood evaluation time also adds to the computational demand of analyzing PTAs. NANOGrav has mitigated this by carrying out single-pulsar noise analyses on each pulsar to determine the white noise parameters before fixing these parameters in a red noise and GW background analysis [Arzoumanian et al., 2016]. Even with these solutions, performing these GW searches still requires a great deal of time. The slowness of traditional Bayesian analyses creates a desire for a faster method of GW analysis. The recent evidence of a common process consistent with expectations of a GW background

in the NANOGrav 12.5 year dataset and others [Arzoumanian et al., 2020] also requires ways of confirming the accuracy of the signal detected in Bayesian methods and tracing its source(s). The Factorized Likelihood approach can satisfy these needs and our work explores the strengths and weaknesses of this method in GW searches, data combination simulation, and cross-validation.

Chapter 2

Statistical Methods

The following description of the PTA Likelihood follows closely from Taylor et al. [2017]. Pulsar timing allows us to measure GWs through deviations in the arrival time of pulsed emissions from an established model. These deviations, or residuals, measure the difference between an observed TOA and a model which predicts the arrival time of the pulsar's radiation at Earth. These timing models include parameters governing the pulsar's position (right ascension, declination, respective proper motions, and parallax), rotation (spin frequency and frequency derivative), and Dispersion Measure (DM) information, which describes the frequency-dependent delay in radiation arrival times due to free electrons in the interstellar medium. This DM parameter can vary over time, especially in the cases when the line-of-sight to the pulsar nears the Sun, encountering the solar wind along the journey to Earth. Keplerian orbital parameters are also included in the pulsar model which govern its orbit if it is in a binary or multi-star system (orbital period, projected semi-major axis, longitude of periastron, epoch of periastron passage, and eccentricity of the orbit). As can be expected, post-Keplerian orbital parameters are included in the rare cases in which relativistic effects cannot be ignored. These systems, in which a pulsar may be interacting with another compact object such as a white dwarf, a neutron star, or a black hole, provide an opportunity to also test strong-field regimes of gravity and thus the ability of General Relativity to predict behaviors. Since these post-Keplerian parameters are solely dependent upon the masses in the system, the measurement of two (or more) parameters will reveal the masses of the pulsar and the companion(s). These post-Keplerian parameters are that of

evolution of the periastron longitude, orbital period time derivative, relativistic orbit deformations, Einstein delay, Shapiro delay, and Geodetic precession. When TOAs are recorded from a pulsar at a given telescope, they must be translated from a topocentric frame which is dependent upon the Earth's position in the Solar System to a barycentric frame which is that of the Solar System Barycenter (SSB). This mitigates the effects of Earth's orbit on the arrival time of the pulses, but this means that the SSB has a large impact on pulsar timing. Assembling an array of well-timed pulsars allows for the measurement of correlated signals within the residuals of multiple pulsars. These signals may be monopolar (clock errors), dipolar (ephemeris errors), or quadrupolar such as those from the GW background.

The PTA Likelihood is composed of the parameter-dependent timing residuals of each pulsar $\delta\mathbf{t}$, the timing model design matrix $\mathbf{M}$, the timing-parameter deviations due to the effects of the GW background ϵ, and the low-frequency processes (intrinsic red noise, common red noise, or the GW background) modeled as as a series of Fourier sums given by the Fourier design matrix $\mathbf{F}$ and their coefficients in $\mathbf{a}$. White noise processes affecting timing residuals are modeled through the inclusion of three key terms: ECORR, EFAC, and EQUAD. TOA measurement uncertainties due to observing backend-specific signals are modeled by the parameters EFAC and EQUAD for each backend. ECORR models the correlated measurement uncertainties due to coordinated multi-wavelength observations, or pulse phase jitter. This gives the following equation for model-dependent timing residuals, $\mathbf{r} = \delta\mathbf{t} - \mathbf{M}\ \epsilon - \mathbf{Fa}$, with a likelihood:

$$p(\delta\mathbf{t}|\epsilon,\ \mathbf{a},\ \eta) = \frac{\exp(-\frac{1}{2}\mathbf{r}^T\mathbf{N}^{-1}\mathbf{r})}{\sqrt{\det(2\pi\mathbf{N})}} \tag{2.1}$$

In this likelihood, $\mathbf{N}$ is the white noise covariance matrix where the effects of marginalized per-pulsar white noise parameters are contained. Further, η represents all parameters not within ϵ or $\mathbf{a}$. The priors on the parameters contained within ϵ and $\mathbf{a}$ are Gaussian in nature, but those of the timing model have an infinite variance due to their uniform unconstrained nature. The low-frequency process parameters in $\mathbf{a}$ are governed by the spectrum of all red noise processes in the data. This variance is given by ϕ which is defined as follows.

$$[\phi]_{(ai),(bj)} = \gamma_{ab}\rho_i\delta_{ij} + \kappa_{ai}\delta_{ab}\delta_{ij} \tag{2.2}$$

In this equation, γ_{ab} is the overlap reduction function (ORF) between pulsars a and b, ρ_i is the GW background spectrum at the ith sampling frequency, and κ_{ai} is the spin noise or intrinsic red noise of pulsar a at the ith sampling frequency. The ORF used in GW background analyses is commonly referred to as the "Hellings and Downs" curve, which describes the correlated power due to the spatial separations of the given pulsars. κ_{ai} and ρ_i are modeled as power laws in our analyses, but ρ_i can also be studied as a power law with a turnover or a free spectrum [Taylor et al., 2017][Hellings and Downs, 1983]. Thus, the cross-power spectral density dictating the delay of pulses due to this background is given by the following equation.

$$S_{ab}(f) = \Gamma_{ab} \times \frac{A_{GW}^2}{12\pi^2} \left(\frac{f}{yr^{-1}}\right)^{-\gamma} yr^3 \tag{2.3}$$

In many analyses in this paper, the 'gw_log$_{10}$_A' parameter is quoted, which is the A_{GW} given in Eq. 2.3. Importantly, this model is dependent on assumptions that the binaries are distributed isotropically, have circular orbits, and that the radiation of GWs is the only process dynamically changing the system [Arzoumanian et al., 2016]. This background can also be described by the characteristic strain

$$h_c(f) = A_{GW} \left(\frac{f}{yr^{-1}}\right)^{\alpha} \tag{2.4}$$

where A_{GW} is the amplitude of the background and $\alpha = -2/3$ is the exponent dictating the power-law background based on a background of SMHBs. This strain can be substituted into Eq. 2.3 as, $S_{ab} = hc^2/(12 \times \pi^2 \times f^3)$, where for $\gamma = 13/3$, $\alpha = -2/3$ [].

The Factorized Likelihood approach serves as a way to bypass the complexities and computational cost of other Bayesian analyses. Its derivation follows from the fact that for a common process without spatial correlations, the PTA likelihood reduces down to a product of pulsar terms. We rederive the Factorized Likelihood following the steps given in Arzoumanian et al. [2020]. The PTA likelihood for a common process is as follows,

$$p\{d_j\}_N|\{\vec{\theta}\}_N, A_{CP}) = \prod_{j=1}^{N} p(d_j|\vec{\theta}_j, A_{CP}) \tag{2.5}$$

where A_{CP} is the amplitude of the common process, d_j is the dataset, and $\vec{\theta_j}$ is the intrinsic noise parameters for the jth pulsar. This means that the posterior for the amplitude of the

common process can be determined by multiplying the individual A_{CP} posteriors for each pulsar. Since this method applies Bayesian frameworks in parallel, it cannot be used in combination with some tools such as BAYESEPHEM.

This Factorized Likelihood method can also be expanded to calculate the dropout ratios that were previously calculated using Bayesian inference. The following derivation was carried out by Dr. Stephen Taylor of Vanderbilt University and is rewritten here for reference. We consider two hypotheses for an array of N pulsars. In $\mathcal{H}_0$, there is intrinsic noise in each pulsar in addition to a common 13/3 spectral-index process. In $\mathcal{H}_1$, there is intrinsic noise in each pulsar, but the common 13/3 spectral-index process in N-1 pulsars. For this hypothesis, the pulsar p does not have a common process present but is included in analyses. The evidence then for H_1, where there is intrinsic noise in each pulsar with an additional 13/3 common process in all pulsars but pulsar p, is:

$$\mathcal{Z}_1 = \int p(\{d\}_{N-1}|\{\vec{\theta}\}_{N-1}, A)p(\{\vec{\theta}\}_{N-1})p(A) \times p(d_p|\vec{\theta}_p)p(\vec{\theta}_p)d^N\{\vec{\theta}\}dA. \tag{2.6}$$

In Eq. 2.6, d is the dataset, $\vec{\theta}$ are intrinsic noise parameters, and A is the amplitude of the common process. This evidence is made up of the Bayes Factor for a $\gamma = 13/3$ common process seen in N-1 pulsars (the first term) and the level of support for this process in pulsar p. We can rewrite one of these terms using Bayes' Theorem,

$$p(\{d\}_{N-1}|\{\vec{\theta}\}_{N-1}, A)p(\{\vec{\theta}\}_{N-1})p(A) = p(A, \{\vec{\theta}\}_{N-1}|\{d\}_{N-1}) \times \mathcal{Z}_*, \tag{2.7}$$

where $\mathcal{Z}_*$ is a normalization term. The intrinsic noise parameters for the (N-1) pulsars in $\mathcal{H}_\infty$ can be marginalized over such that,

$$\mathcal{Z}_1 = \mathcal{Z}_* \times \int p(A\{\vec{\theta}\}_{N-1}|\{d\}_{N-1}) \times p(d_p|\vec{\theta_p})p(\vec{\theta_p})d\vec{\theta}_p dA \tag{2.8}$$

$$= \mathcal{Z}_* \times \int p(A|\mathcal{H}_\infty)dA \times \int p(d_p|\vec{\theta_p})p(\vec{\theta_p})d\vec{\theta_p} \tag{2.9}$$

$$= \mathcal{Z}_* \times \mathcal{Z}_{p,0} \tag{2.10}$$

where the integration of $p(A|\mathcal{H}_1)$ gives one and the integral over pulsar p's returns the evidence $\mathcal{Z}_{p,0}$. Following these steps again for $\mathcal{H}_0$, we find:

$$\mathcal{Z}_0 = \mathcal{Z}_* \times \int p(A\{\vec{\theta}\}_{N-1}|\{d\}_{N-1}) \times p(d_p|\vec{\theta_p}, A)p(\vec{\theta_p})d\vec{\theta_p}dA \tag{2.11}$$

$$= \mathcal{Z}_* \times \int p(A|\mathcal{H}_\infty) \times p(d_p|\vec{\theta_p}, A)p(\vec{\theta_p})d\vec{\theta_p}dA \tag{2.12}$$

$$= \mathcal{Z}_* \times \int \frac{p(A|\mathcal{H}_1)}{p(A)} \times p(d_p|\vec{\theta_p}, A)p(\vec{\theta_p})p(A)d\vec{\theta_p}dA \tag{2.13}$$

$$= \mathcal{Z}_* \times \mathcal{Z}_p \times \int \frac{p(A|\mathcal{H}_1)}{p(A)} \times p(A, \vec{\theta_p}|d_p)d\vec{\theta_p}dA \tag{2.14}$$

$$= \mathcal{Z}_* \times \mathcal{Z}_p \times \left\langle \frac{p(A|\mathcal{H}_1)}{p(A)} \right\rangle_p \tag{2.15}$$

Thus, to determine the ratio of evidences between hypothesis 0, where the common process is present in pulsar p, and 1, where the common process is absent from pulsar p, we divide the evidences.

$$\frac{\mathcal{Z}_0}{\mathcal{Z}_1} = \frac{\mathcal{Z}_p}{\mathcal{Z}_{p,0}} \left\langle \frac{p(A|\mathcal{H}_1)}{p(A)} \right\rangle_p \tag{2.16}$$

In Eq. 2.16, $p(A|\mathcal{H}_1)$ is the support for the common process in the PTA without pulsar p, $p(A)$ is the uniform log prior which restricts the common process search, and the ratio of these two is averaged over pulsar p's common process. This quantity is then multiplied by the ratio of evidences for pulsar p ($\mathcal{Z}_p$ being the evidence for the common process in pulsar p and $\mathcal{Z}_{p,0}$ being the evidence for pulsar p showing only intrinsic noise and no common process). This final ratio of Bayesian evidences is the dropout ratio for a given pulsar p that is calculated through the Factorized Likelihood approach rather than Bayesian inference techniques using MCMC. The dropout factor calculated through the Factorized Likelihood method, however, does not have uncertainties like those determined through Bayesian MCMC runs. To obtain uncertainties for the dropout parameter, we make use of the Bootstrapping statistical procedure [Efron and Tibshirani, 1994]. In this procedure, the posteriors for the common process amplitude of each pulsar are resampled with replacement, such that the true posterior is re-appproximated. The bootstrapped-posteriors for every pulsar in the array are then used to calculate dropout ratios for all the pulsars. This process is repeated so, after enough iterations, a standard deviation can be calculated for each pulsar's dropout ratio.

By searching for the evidence of GWs in each pulsar and then creating the PTA afterward through the Factorized Likelihood, analyses can be completed quickly. The modular

characteristics of the assembled PTA also allow for quick experimentation and exploration of dynamics within the dataset. This means that tests to explore the evidence for the GW background within a subset of the pulsars is incredibly trivial to perform and quantify using the quick dropout factor.

Chapter 3

The Datasets

To explore the capabilities of the Factorized Likelihood method to simulate an entire PTA, we began by using only PSR J1713+0747 (hereafter J1713). This pulsar was chosen because it has one of the longest baselines in IPTADR2, it is observed by NANOGrav, the EPTA, and PPTA, and it has a strong red noise process. With this pulsar chosen, we carried out single pulsar analyses with the same parameters to explore the performance of different datasets. We used the Enterprise GW analysis software along with Enterprise_Extensions [Taylor et al., 2018] to create a PTA consisting of only J1713 which allowed the DM parameters to be searched over, used white noise parameters supplied by Dr. Siyuan Chen, an intrinsic red noise process, and finally a common red noise process modeled as a power law with $\gamma = 13/3$ using the default 30 frequencies and the timespan of the full array. This common red noise process is to explore for the effects of a GW amplitude on the residuals of J1713, but the intrinsic red noise process is to model low frequency noise apparent in some residuals that are specific to the pulsar, but uncorrelated across the array. This PTA likelihood was then sampled using Markov-Chain Monte Carlo (MCMC) sampling to determine the posterior distributions of the parameters governing the different noise processes added. This analysis was performed on several different versions of J1713 from the different datasets. We first analyzed IPTADR2 and the constituent datasets of the NANOGrav 9-year, EPTA Data Release 1, and the PPTA Data Release 1 extended (NG9, EPTADR1, and PPTADR1e hereafter respectively). With the posteriors for the 'GW_log$_{10}$_A' from these runs we were able to test the Factorized Likelihood approach's ability to approximate a meticulous data

combination. For the NG9 dataset, we performed two analyses. To model the time evolution of DM, NANOGrav utilizes epoch-dependent DM offsets or DMX parameters, but the EPTA and PPTA use Gaussian-process models with parameters DM1 and DM2. Taking this into account, we performed the single pulsar analysis using the NG9 J1713 once using the DMX parameter, not allowing the DM values to vary, and once removing the DMX parameters and utilizing the DM1 and DM2 parameters. These two analyses produced consistent posteriors, which gave us confidence in the results from the analysis using DM1 and DM2. The posteriors for the constituent datasets were multiplied through the Factorized Likelihood method to simulate IPTADR2. A plot of these posteriors and the 'quasi-IPTA' created through the Factorized Likelihood is in Fig. 3.1.

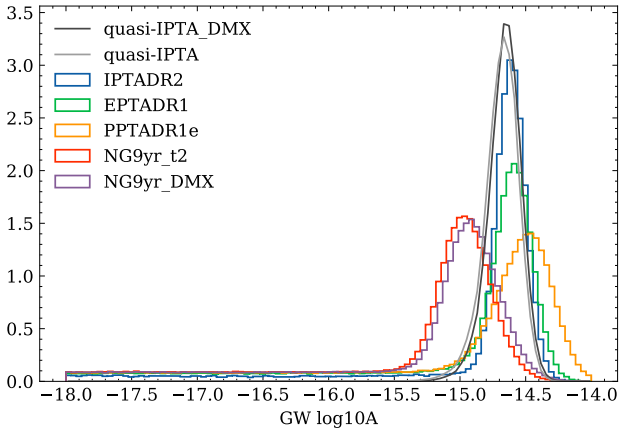

Figure 3.1: A plot of the GW $\log_{10}$ Amplitude parameter sampled from ENTERPRISE single pulsar runs of J1713. In this plot the posteriors of constituent datasets are compared to that of the full IPTADR2, and the Factorized Likelihood product is displayed.

We then created PTA-specific datasets by filtering TOAs out of IPTADR2 while continuing to use the original parameter file included with the data release. These datasets are referenced as filtered NG, EP, and PP hereafter. These filtered datasets were made in an attempt to recreate the original constituent datasets and see how the data combination process affected the input data. The filtering was carried out by the dr2utils [Baker, 2019] software developed by Dr. Paul Baker. These new filtered datasets were again used to perform identical single pulsar analyses as that of the constituent datasets. Again, their factorized likelihood product was created from the posteriors of their GW amplitude param-

eter. A plot comparing these datasets is in Fig 3.2. Although these datasets were expected to be consistent with consituent ones, discrepancies were noticed between this dataset and the constituent datasets. These discrepancies are discussed in Section 4.

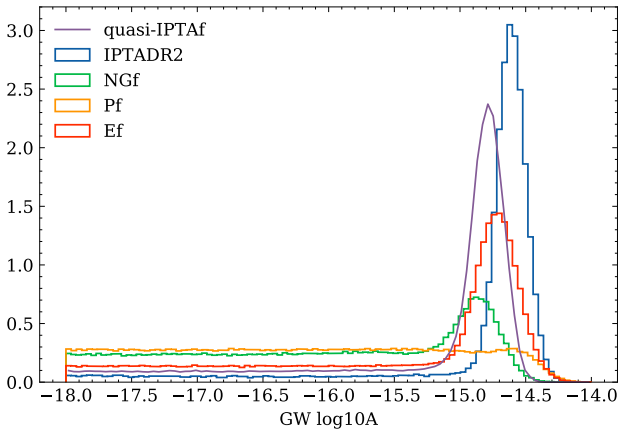

Figure 3.2: A plot of the GW $\log_{10}$ Amplitude parameter sampled from ENTERPRISE single pulsar runs of J1713. In this plot the posteriors of filter datasets are compared to that of the full IPTADR2, and the Factorized Likelihood product is displayed.

We also developed a new approach to single pulsar analyses specifically to explore data combination forecasting. This method, referred to as a Borg [1] analysis, involved creating a three-pulsar PTA from the constituent versions of J1713. Since this seemingly multi-pulsar array was in actuality the same pulsar, new noise processes had to be constructed. These parameters were a common DM (including a common DM process to account for the first interstellar medium event experienced by J1713), common intrinsic red noise, and common GW amplitude which added to the model_general software within Enterprise_Extensions. Since the GW amplitude parameter is common across the PTA, the Factorized Likelihood approach is not necessary for analysis; a single posterior is the result. These posteriors are shown in Fig. 3.3.

The Borg analysis was also carried out on another well-timed pulsar observed by all three PTAs, PSR J1909-3744 (hereafter J1909). For comparison to IPTADR2, a standard single pulsar analysis was performed on J1909 as well. These results can be seen in Fig. 3.4.

IPTADR2 also has yet to be extensively searched for evidence of GWs, so we carried out

[1] https://en.wikipedia.org/wiki/Borg

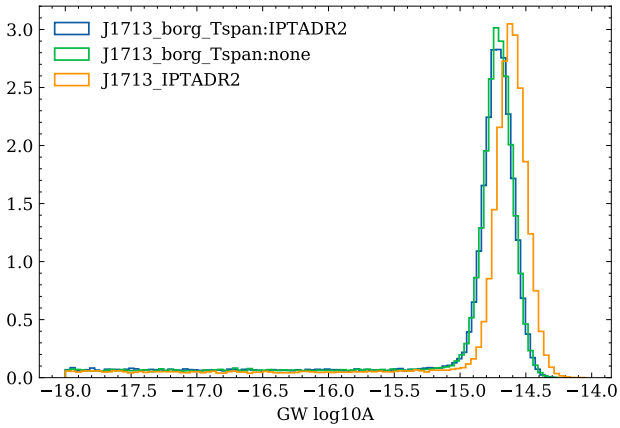

Figure 3.3: A plot of the GW $\log_{10}$ Amplitude parameter sampled from the newly developed Borg analysis. In this plot the posteriors of borg datasets using J1713 with different timespans specified for the common process sampling are compared to that of the IPTADR2 version of J1713.

these single pulsar analyses on all 65 pulsars in the array. These analyses were performed using 5, 10, 13, and 30 frequencies modeling the GW background. For the 13 frequency analysis, empirical red noise distributions were used as well as modified parameter files with timing noise parameters removed. These analyses were performed in parallel on high-performance computing resources at West Virginia University. These chains were used to perform dropout analyses on IPTADR2, determining the level of support in each pulsar for the common process seen by the rest of the array. These dropout ratios were calculated using the Factorized Likelihood approach. These chains were also used in cross validation tests by splitting the IPTA into different subarrays to compare their evidences of GWs. One such subarray was removing pulsars that had baselines shorter than three years.

While this work on IPTADR2 was being performed, the NANOGrav collaboration was preparing new versions of its premier 15-year dataset. We performed a 5-frequency dropout analysis on one such dataset, prelim1, using the same methods as those used for IPTADR2. Dr. Nihan Pol also supplied chains for 5, 10, and 30 frequency single pulsar analyses for prelim1 and v0 which we also used in Dropout analyses. In v0, we only studied the pulsars observed by the GBT, as those observed with the Arecibo Observatory displayed problematic behavior as a result of the malfunctioning local oscillator at the observatory. A Dropout

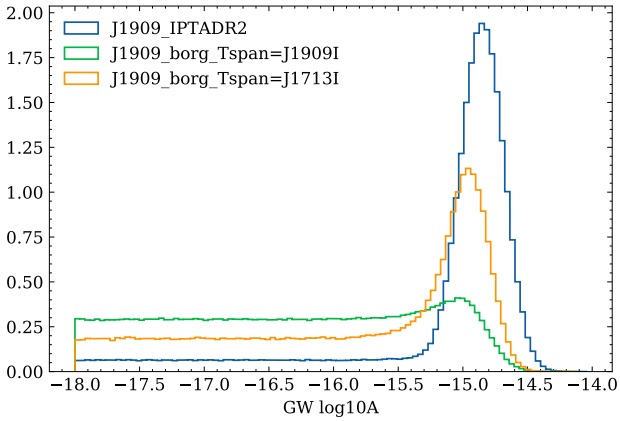

Figure 3.4: A plot of the GW $\log_{10}$ Amplitude parameter sampled from the Borg analysis. In this plot the posteriors of borg datasets using J1909 with different timespans specified for the common process sampling are compared to that of the IPTADR2 version of J1909.

analysis was also curated such that it used the v0 pulsars where possible and prelim1 pulsars otherwise. In this analysis, the v0 pulsars were PSRs J1909-3744, J1615-2230, J1832-0836, J0613-0200, J1744-1134, J1918-0642, J2010-1323, J1455-3330, and J1600-3053. A plot of these results can be found in Fig. 3.6.

Uncertainties for these Factorized Likelihood dropout ratios were calculated by utilizing bootstrap statistical methods. The GW amplitude chain for each pulsar had a burn in length removed (burn in was uniformly determined as a quarter of the total chain length) and thinned by the autocorrelation length. This chain was then resampled with replacement to create a new chain with a length equal to the original. These new chains were then used to calculate dropout ratios for all the pulsars in the array. For PSR J1713, the tolerance factor for calculating its Bayes Factor had to be reduced to produce an acceptable calculation of its dropout ratio. This is due to the highly constrained posterior of J1713 on the GW amplitude. This process was carried out 1000 times to create a strong statistical sample before the median, mean, and standard deviation of the bootstrapped dropout ratios was calculated. The median and mean dropout ratio for each pulsar was used to confirm the accuracy of the dropout ratio calculated using the un-thinned original chain, and the standard deviation was used as its uncertainty. These dropout ratios with accompanying uncertainties can be found in Fig. 3.5.

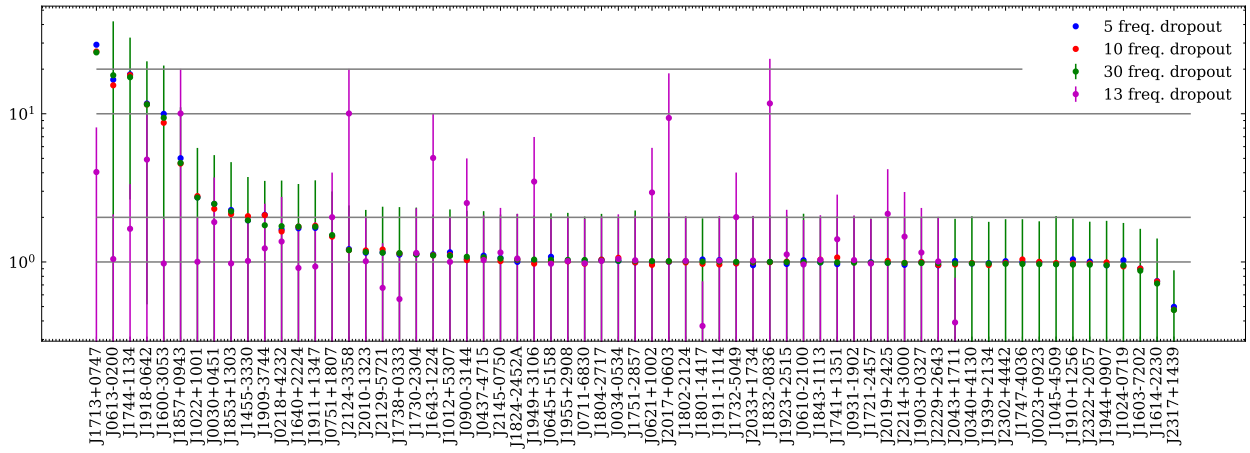

Figure 3.5: A plot of the dropout ratios for the pulsars in IPTADR2 using different frequencies for sampling the common process. The uncertainties for the 30 and 13 frequency run are given. The 13 frequency run included only pulsars with baselines greater than 3 years, so excluded pulsars were given a dropout ratio of 0.

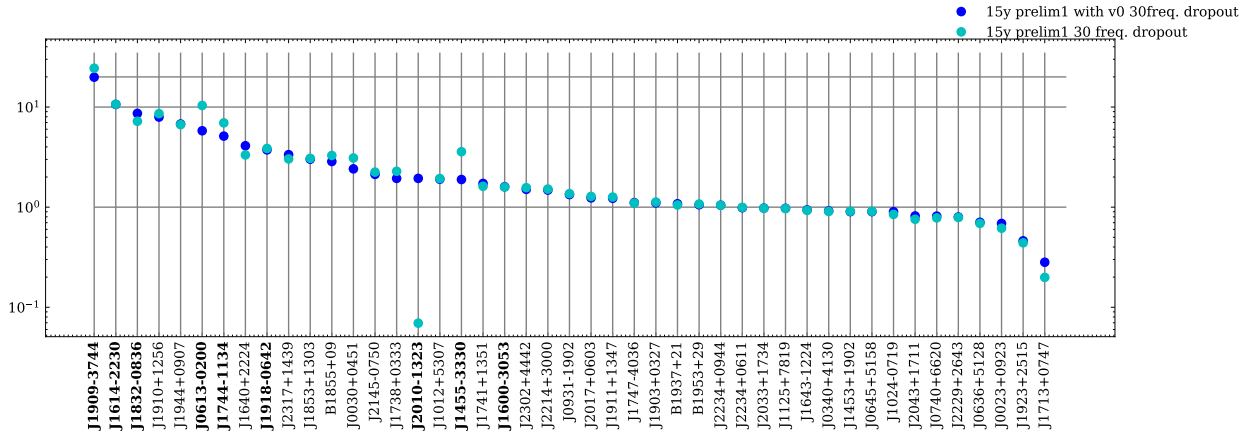

Figure 3.6: A plot of the dropout ratios for the pulsars in the NANOGrav 15-year prelim1 dataset and the same analysis performed with the v0 versions of selected pulsars. Bolded pulsar names indicate usage of the v0 dataset in this analysis. Only pulsars observed at the GBT were used in this v0 implementation due to timing solution problems related to the hardware issues at Arecibo Observatory.

Chapter 4

Discussion and Results

Multiplying the posteriors for the GW amplitude of the NG9, EPTADR1, and PPTADR1e versions of J1713, we found that using the factorized likelihood approach produced remarkably similar results to that of the fully combined IPTADR2. Although this is a preliminary result, it is extremely promising for the future of the IPTA. If these trends continue when the analysis is carried out on the full IPTADR2, then it would mean that the dataset combination process could be optimized. We could pick which datasets to combine to achieve the most sensitive detector yet. The ability to forecast the abilities of a combined dataset would also motivate the tedious and painstaking efforts required in IPTA data combinations.

The Factorized Likelihood results for the filtered datasets are difficult to interpret. Startlingly, the posteriors for the PTAs are drastically different to their constituent counterparts. This discrepancy somewhat explains the difference between the filtered and constituent dataset results. One such reason may be the inclusion of legacy data for NANOGrav and the PPTA in their addition to IPTADR2, but this theory has not been robustly tested.

The Borg analyses showed extremely promising results with J1713, but J1909's raised more questions. For J1713, the GW amplitude posterior was very consistent with that of IPTADR2 and even moreso when using the timespan of J1713 rather than that of the full array. This trend was reversed in the case of J1909, where the use of J1713's timespan produced (This was an accident in the analysis process, and the J1713 timespan is approximately double J1909's) a posterior that was closer to the IPTADR2 result. These results are extremely preliminary as well, since there are more tools that are required to properly

carry out this Borg analysis, including a common timing model across the datasets. In the current method, the timing models of each version of the selected pulsar are marginalized over, rather than incorporating them together.

The Dropout results from IPTADR2 point to the reward of the strenuous data combination process. The GW signal detected in IPTADR2 with these analyses rivals that of datasets that being developed now, highlighting their importance. Results were consistent with Dropout ratios derived using the Hypermodel approach except in the case of PSR J1909. In Hypermodel analyses, J1909 does not support the presence of a common red noise process and instead refutes it strongly. In our Factorized Likelihood approach, J1909's dropout ratio is one of the highest, suggesting strong evidence for the GW background. The source of this disagreement between the two methods has not been determined yet but is actively being investigated. This behavior motivated the development of the bootstrap derivation of Factorized Likelihood dropout ratio uncertainties. These uncertainties may resolve the disagreement between the two methods for deriving a dropout ratio.

Chapter 5

Future Work

These studies were initial explorations into the potential of the Factorized Likelihood approach. The results thus far motivate future work expanding these analyses to all the pulsars in IPTADR2 rather than only J1713 or J1909. This would allow us to further characterize the utility of the Factorized Likelihood method. For the filter datasets, we are working to robustly remove NANOGrav and PPTA legacy data from IPTADR2 to create a dataset that we expect to be equivalent to the constituent datasets. Tests on these filter datasets without legacy data could illuminate further the modifications that are present in the data combination process to create IPTADR2.

As alluded to previously, the Borg method is incomplete in its present state. Although the pulsar-specific common red noise and common DM noise processes were added, the timing models for the different versions of the pulsar are independent. Without implementing a common timing model across the pulsars used, each is marginalized over, reducing the sensitivity of the array. We would like to develop this and other features for the Borg method in the future as well.

The dropout ratios calculated in this work will serve as a cross-validation technique in an upcoming paper focused on analyzing IPTADR2 for evidence of GWs. We are interested in developing the subarray methods to have another informative, quick approach to probe the performance of NANOGrav and other PTAs. We also aim to parse through pulsar metadata and quantify the dropout ratio in terms of other known pulsar parameters.

Bibliography

Steven Detweiler. Pulsar timing measurements and the search for gravitational waves. *The Astrophysical Journal*, 234:1100–1104, 1979. 1

Roger Sherman Foster and DC Backer. Constructing a pulsar timing array. *The Astrophysical Journal*, 361:300–308, 1990. 1

M Bailes, BK Berger, PR Brady, M Branchesi, K Danzmann, M Evans, K Holley-Bockelmann, BR Iyer, T Kajita, S Katsanevas, et al. Gravitational-wave physics and astronomy in the 2020s and 2030s. *Nature Reviews Physics*, pages 1–23, 2021. 1

Pablo A. Rosado, Alberto Sesana, and Jonathan Gair. Expected properties of the first gravitational wave signal detected with pulsar timing arrays. , 451(3):2417–2433, August 2015. doi: 10.1093/mnras/stv1098. 1

Joseph D Romano, Jeffrey S Hazboun, Xavier Siemens, and Anne M Archibald. Common-spectrum process versus cross-correlation for gravitational-wave searches using pulsar timing arrays. *Physical Review D*, 103(6):063027, 2021. 1

R. W. Hellings and G. S. Downs. Upper limits on the isotropic gravitational radiation background from pulsar timing analysis. , 265:L39–L42, February 1983. doi: 10.1086/183954. 1, 2

B. P. Abbott, R. Abbott, T. D. Abbott, M. R. Abernathy, F. Acernese, K. Ackley, C. Adams, T. Adams, P. Addesso, R. X. Adhikari, V. B. Adya, C. Affeldt, M. Agathos, K. Agatsuma, N. Aggarwal, O. D. Aguiar, L. Aiello, A. Ain, P. Ajith, B. Allen, A. Allocca, P. A. Altin, S. B. Anderson, W. G. Anderson, K. Arai, M. C. Araya, C. C. Arceneaux,

J. S. Areeda, N. Arnaud, K. G. Arun, S. Ascenzi, G. Ashton, M. Ast, S. M. Aston, P. Astone, P. Aufmuth, C. Aulbert, S. Babak, P. Bacon, M. K. M. Bader, P. T. Baker, F. Baldaccini, G. Ballardin, S. W. Ballmer, J. C. Barayoga, S. E. Barclay, B. C. Barish, D. Barker, F. Barone, B. Barr, L. Barsotti, M. Barsuglia, D. Barta, J. Bartlett, I. Bartos, R. Bassiri, A. Basti, J. C. Batch, C. Baune, V. Bavigadda, M. Bazzan, M. Bejger, A. S. Bell, B. K. Berger, G. Bergmann, C. P. L. Berry, D. Bersanetti, A. Bertolini, J. Betzwieser, S. Bhagwat, R. Bhandare, I. A. Bilenko, G. Billingsley, J. Birch, R. Birney, O. Birnholtz, S. Biscans, A. Bisht, M. Bitossi, C. Biwer, M. A. Bizouard, J. K. Blackburn, C. D. Blair, D. G. Blair, R. M. Blair, S. Bloemen, O. Bock, M. Boer, G. Bogaert, C. Bogan, A. Bohe, C. Bond, F. Bondu, R. Bonnand, B. A. Boom, R. Bork, V. Boschi, S. Bose, Y. Bouffanais, A. Bozzi, C. Bradaschia, P. R. Brady, V. B. Braginsky, M. Branchesi, J. E. Brau, T. Briant, A. Brillet, M. Brinkmann, V. Brisson, P. Brockill, J. E. Broida, A. F. Brooks, D. A. Brown, D. D. Brown, N. M. Brown, S. Brunett, C. C. Buchanan, A. Buikema, T. Bulik, H. J. Bulten, A. Buonanno, D. Buskulic, C. Buy, R. L. Byer, M. Cabero, L. Cadonati, G. Cagnoli, C. Cahillane, J. Calderón Bustillo, T. Callister, E. Calloni, J. B. Camp, K. C. Cannon, J. Cao, C. D. Capano, E. Capocasa, F. Carbognani, S. Caride, J. Casanueva Diaz, C. Casentini, S. Caudill, M. Cavaglià, F. Cavalier, R. Cavalieri, G. Cella, C. B. Cepeda, L. Cerboni Baiardi, G. Cerretani, E. Cesarini, S. J. Chamberlin, M. Chan, S. Chao, P. Charlton, E. Chassande-Mottin, B. D. Cheeseboro, H. Y. Chen, Y. Chen, C. Cheng, A. Chincarini, A. Chiummo, H. S. Cho, M. Cho, J. H. Chow, N. Christensen, Q. Chu, S. Chua, S. Chung, G. Ciani, F. Clara, J. A. Clark, F. Cleva, E. Coccia, P. F. Cohadon, A. Colla, C. G. Collette, L. Cominsky, M. Constancio, A. Conte, L. Conti, D. Cook, T. R. Corbitt, N. Cornish, A. Corsi, S. Cortese, C. A. Costa, M. W. Coughlin, S. B. Coughlin, J. P. Coulon, S. T. Countryman, P. Couvares, E. E. Cowan, D. M. Coward, M. J. Cowart, D. C. Coyne, R. Coyne, K. Craig, J. D. E. Creighton, J. Cripe, S. G. Crowder, A. Cumming, L. Cunningham, E. Cuoco, T. Dal Canton, S. L. Danilishin, S. D'Antonio, K. Danzmann, N. S. Darman, A. Dasgupta, C. F. Da Silva Costa, V. Dattilo, I. Dave, M. Davier, G. S. Davies, E. J. Daw, R. Day, S. De, D. DeBra, G. Debreczeni, J. Degallaix, M. De Laurentis, S. Deléglise, W. Del Pozzo, T. Denker, T. Dent, V. Dergachev, R. De Rosa, R. T. DeRosa, R. DeSalvo, R. C. Devine, S. Dhurandhar, M. C. Díaz, L. Di Fiore, M. Di

Giovanni, T. Di Girolamo, A. Di Lieto, S. Di Pace, I. Di Palma, A. Di Virgilio, V. Dolique, F. Donovan, K. L. Dooley, S. Doravari, R. Douglas, T. P. Downes, M. Drago, R. W. P. Drever, J. C. Driggers, M. Ducrot, S. E. Dwyer, T. B. Edo, M. C. Edwards, A. Effler, H. B. Eggenstein, P. Ehrens, J. Eichholz, S. S. Eikenberry, W. Engels, R. C. Essick, T. Etzel, M. Evans, T. M. Evans, R. Everett, M. Factourovich, V. Fafone, H. Fair, S. Fairhurst, X. Fan, Q. Fang, S. Farinon, B. Farr, W. M. Farr, M. Favata, M. Fays, H. Fehrmann, M. M. Fejer, E. Fenyvesi, I. Ferrante, E. C. Ferreira, F. Ferrini, F. Fidecaro, I. Fiori, D. Fiorucci, R. P. Fisher, R. Flaminio, M. Fletcher, H. Fong, J. D. Fournier, S. Frasca, F. Frasconi, Z. Frei, A. Freise, R. Frey, V. Frey, P. Fritschel, V. V. Frolov, P. Fulda, M. Fyffe, H. A. G. Gabbard, S. Gaebel, J. R. Gair, L. Gammaitoni, S. G. Gaonkar, F. Garufi, G. Gaur, N. Gehrels, G. Gemme, P. Geng, E. Genin, A. Gennai, J. George, L. Gergely, V. Germain, Abhirup Ghosh, Archisman Ghosh, S. Ghosh, J. A. Giaime, K. D. Giardina, A. Giazotto, K. Gill, A. Glaefke, E. Goetz, R. Goetz, L. Gondan, G. González, J. M. Gonzalez Castro, A. Gopakumar, N. A. Gordon, M. L. Gorodetsky, S. E. Gossan, M. Gosselin, R. Gouaty, A. Grado, C. Graef, P. B. Graff, M. Granata, A. Grant, S. Gras, C. Gray, G. Greco, A. C. Green, P. Groot, H. Grote, S. Grunewald, G. M. Guidi, X. Guo, A. Gupta, M. K. Gupta, K. E. Gushwa, E. K. Gustafson, R. Gustafson, J. J. Hacker, B. R. Hall, E. D. Hall, H. Hamilton, G. Hammond, M. Haney, M. M. Hanke, J. Hanks, C. Hanna, M. D. Hannam, J. Hanson, T. Hardwick, J. Harms, G. M. Harry, I. W. Harry, M. J. Hart, M. T. Hartman, C. J. Haster, K. Haughian, J. Healy, A. Heidmann, M. C. Heintze, H. Heitmann, P. Hello, G. Hemming, M. Hendry, I. S. Heng, J. Hennig, J. Henry, A. W. Heptonstall, M. Heurs, S. Hild, D. Hoak, D. Hofman, K. Holt, D. E. Holz, P. Hopkins, J. Hough, E. A. Houston, E. J. Howell, Y. M. Hu, S. Huang, E. A. Huerta, D. Huet, B. Hughey, S. Husa, S. H. Huttner, T. Huynh-Dinh, N. Indik, D. R. Ingram, R. Inta, H. N. Isa, J. M. Isac, M. Isi, T. Isogai, B. R. Iyer, K. Izumi, T. Jacqmin, H. Jang, K. Jani, P. Jaranowski, S. Jawahar, L. Jian, F. Jiménez-Forteza, W. W. Johnson, N. K. Johnson-McDaniel, D. I. Jones, R. Jones, R. J. G. Jonker, L. Ju, Haris K, C. V. Kalaghatgi, V. Kalogera, S. Kandhasamy, G. Kang, J. B. Kanner, S. J. Kapadia, S. Karki, K. S. Karvinen, M. Kasprzack, E. Katsavounidis, W. Katzman, S. Kaufer, T. Kaur, K. Kawabe, F. Kéfélian, M. S. Kehl, D. Keitel, D. B. Kelley, W. Kells, R. Kennedy, J. S. Key, F. Y.

Khalili, I. Khan, S. Khan, Z. Khan, E. A. Khazanov, N. Kijbunchoo, Chi-Woong Kim, Chunglee Kim, J. Kim, K. Kim, N. Kim, W. Kim, Y. M. Kim, S. J. Kimbrell, E. J. King, P. J. King, J. S. Kissel, B. Klein, L. Kleybolte, S. Klimenko, S. M. Koehlenbeck, S. Koley, V. Kondrashov, A. Kontos, M. Korobko, W. Z. Korth, I. Kowalska, D. B. Kozak, V. Kringel, B. Krishnan, A. Królak, C. Krueger, G. Kuehn, P. Kumar, R. Kumar, L. Kuo, A. Kutynia, B. D. Lackey, M. Landry, J. Lange, B. Lantz, P. D. Lasky, M. Laxen, A. Lazzarini, C. Lazzaro, P. Leaci, S. Leavey, E. O. Lebigot, C. H. Lee, H. K. Lee, H. M. Lee, K. Lee, A. Lenon, M. Leonardi, J. R. Leong, N. Leroy, N. Letendre, Y. Levin, J. B. Lewis, T. G. F. Li, A. Libson, T. B. Littenberg, N. A. Lockerbie, A. L. Lombardi, L. T. London, J. E. Lord, M. Lorenzini, V. Loriette, M. Lormand, G. Losurdo, J. D. Lough, C. Lousto, H. Lück, A. P. Lundgren, R. Lynch, Y. Ma, B. Machenschalk, M. MacInnis, D. M. Macleod, F. Magaña-Sandoval, L. Magaña Zertuche, R. M. Magee, E. Majorana, I. Maksimovic, V. Malvezzi, N. Man, I. Mandel, V. Mandic, V. Mangano, G. L. Mansell, M. Manske, M. Mantovani, F. Marchesoni, F. Marion, S. Márka, Z. Márka, A. S. Markosyan, E. Maros, F. Martelli, L. Martellini, I. W. Martin, D. V. Martynov, J. N. Marx, K. Mason, A. Masserot, T. J. Massinger, M. Masso-Reid, S. Mastrogiovanni, F. Matichard, L. Matone, N. Mavalvala, N. Mazumder, R. McCarthy, D. E. McClelland, S. McCormick, S. C. McGuire, G. McIntyre, J. McIver, D. J. McManus, T. McRae, S. T. McWilliams, D. Meacher, G. D. Meadors, J. Meidam, A. Melatos, G. Mendell, R. A. Mercer, E. L. Merilh, M. Merzougui, S. Meshkov, C. Messenger, C. Messick, R. Metzdorff, P. M. Meyers, F. Mezzani, H. Miao, C. Michel, H. Middleton, E. E. Mikhailov, L. Milano, A. L. Miller, A. Miller, B. B. Miller, J. Miller, M. Millhouse, Y. Minenkov, J. Ming, S. Mirshekari, C. Mishra, S. Mitra, V. P. Mitrofanov, G. Mitselmakher, R. Mittleman, A. Moggi, M. Mohan, S. R. P. Mohapatra, M. Montani, B. C. Moore, C. J. Moore, D. Moraru, G. Moreno, S. R. Morriss, K. Mossavi, B. Mours, C. M. Mow-Lowry, G. Mueller, A. W. Muir, Arunava Mukherjee, D. Mukherjee, S. Mukherjee, N. Mukund, A. Mullavey, J. Munch, D. J. Murphy, P. G. Murray, A. Mytidis, I. Nardecchia, L. Naticchioni, R. K. Nayak, K. Nedkova, G. Nelemans, T. J. N. Nelson, M. Neri, A. Neunzert, G. Newton, T. T. Nguyen, A. B. Nielsen, S. Nissanke, A. Nitz, F. Nocera, D. Nolting, M. E. N. Normandin, L. K. Nuttall, J. Oberling, E. Ochsner, J. O'Dell, E. Oelker, G. H. Ogin, J. J. Oh, S. H. Oh,

F. Ohme, M. Oliver, P. Oppermann, Richard J. Oram, B. O'Reilly, R. O'Shaughnessy, D. J. Ottaway, H. Overmier, B. J. Owen, A. Pai, S. A. Pai, J. R. Palamos, O. Palashov, C. Palomba, A. Pal-Singh, H. Pan, Y. Pan, C. Pankow, F. Pannarale, B. C. Pant, F. Paoletti, A. Paoli, M. A. Papa, H. R. Paris, W. Parker, D. Pascucci, A. Pasqualetti, R. Passaquieti, D. Passuello, B. Patricelli, Z. Patrick, B. L. Pearlstone, M. Pedraza, R. Pedurand, L. Pekowsky, A. Pele, S. Penn, A. Perreca, L. M. Perri, H. P. Pfeiffer, M. Phelps, O. J. Piccinni, M. Pichot, F. Piergiovanni, V. Pierro, G. Pillant, L. Pinard, I. M. Pinto, M. Pitkin, M. Poe, R. Poggiani, P. Popolizio, E. Porter, A. Post, J. Powell, J. Prasad, V. Predoi, T. Prestegard, L. R. Price, M. Prijatelj, M. Principe, S. Privitera, R. Prix, G. A. Prodi, L. Prokhorov, O. Puncken, M. Punturo, P. Puppo, M. Pürrer, H. Qi, J. Qin, S. Qiu, V. Quetschke, E. A. Quintero, R. Quitzow-James, F. J. Raab, D. S. Rabeling, H. Radkins, P. Raffai, S. Raja, C. Rajan, M. Rakhmanov, P. Rapagnani, V. Raymond, M. Razzano, V. Re, J. Read, C. M. Reed, T. Regimbau, L. Rei, S. Reid, D. H. Reitze, H. Rew, S. D. Reyes, F. Ricci, K. Riles, M. Rizzo, N. A. Robertson, R. Robie, F. Robinet, A. Rocchi, L. Rolland, J. G. Rollins, V. J. Roma, J. D. Romano, R. Romano, G. Romanov, J. H. Romie, D. Rosińska, S. Rowan, A. Rüdiger, P. Ruggi, K. Ryan, S. Sachdev, T. Sadecki, L. Sadeghian, M. Sakellariadou, L. Salconi, M. Saleem, F. Salemi, A. Samajdar, L. Sammut, E. J. Sanchez, V. Sandberg, B. Sandeen, J. R. Sanders, B. Sassolas, B. S. Sathyaprakash, P. R. Saulson, O. E. S. Sauter, R. L. Savage, A. Sawadsky, P. Schale, R. Schilling, J. Schmidt, P. Schmidt, R. Schnabel, R. M. S. Schofield, A. Schönbeck, E. Schreiber, D. Schuette, B. F. Schutz, J. Scott, S. M. Scott, D. Sellers, A. S. Sengupta, D. Sentenac, V. Sequino, A. Sergeev, Y. Setyawati, D. A. Shaddock, T. Shaffer, M. S. Shahriar, M. Shaltev, B. Shapiro, P. Shawhan, A. Sheperd, D. H. Shoemaker, D. M. Shoemaker, K. Siellez, X. Siemens, M. Sieniawska, D. Sigg, A. D. Silva, A. Singer, L. P. Singer, A. Singh, R. Singh, A. Singhal, A. M. Sintes, B. J. J. Slagmolen, J. R. Smith, N. D. Smith, R. J. E. Smith, E. J. Son, B. Sorazu, F. Sorrentino, T. Souradeep, A. K. Srivastava, A. Staley, M. Steinke, J. Steinlechner, S. Steinlechner, D. Steinmeyer, B. C. Stephens, S. Stevenson, R. Stone, K. A. Strain, N. Straniero, G. Stratta, N. A. Strauss, S. Strigin, R. Sturani, A. L. Stuver, T. Z. Summerscales, L. Sun, S. Sunil, P. J. Sutton, B. L. Swinkels, M. J. Szczepańczyk, M. Tacca, D. Talukder, D. B. Tanner, M. Tápai,

S. P. Tarabrin, A. Taracchini, R. Taylor, T. Theeg, M. P. Thirugnanasambandam, E. G. Thomas, M. Thomas, P. Thomas, K. A. Thorne, E. Thrane, S. Tiwari, V. Tiwari, K. V. Tokmakov, K. Toland, C. Tomlinson, M. Tonelli, Z. Tornasi, C. V. Torres, C. I. Torrie, D. Töyrä, F. Travasso, G. Traylor, D. Trifirò, M. C. Tringali, L. Trozzo, M. Tse, M. Turconi, D. Tuyenbayev, D. Ugolini, C. S. Unnikrishnan, A. L. Urban, S. A. Usman, H. Vahlbruch, G. Vajente, G. Valdes, M. Vallisneri, N. van Bakel, M. van Beuzekom, J. F. J. van den Brand, C. Van Den Broeck, D. C. Vander-Hyde, L. van der Schaaf, J. V. van Heijningen, A. A. van Veggel, M. Vardaro, S. Vass, M. Vasúth, R. Vaulin, A. Vecchio, G. Vedovato, J. Veitch, P. J. Veitch, K. Venkateswara, D. Verkindt, F. Vetrano, A. Viceré, S. Vinciguerra, D. J. Vine, J. Y. Vinet, S. Vitale, T. Vo, H. Vocca, C. Vorvick, D. V. Voss, W. D. Vousden, S. P. Vyatchanin, A. R. Wade, L. E. Wade, M. Wade, M. Walker, L. Wallace, S. Walsh, G. Wang, H. Wang, M. Wang, X. Wang, Y. Wang, R. L. Ward, J. Warner, M. Was, B. Weaver, L. W. Wei, M. Weinert, A. J. Weinstein, R. Weiss, L. Wen, P. Weßels, T. Westphal, K. Wette, J. T. Whelan, S. E. Whitcomb, B. F. Whiting, R. D. Williams, A. R. Williamson, J. L. Willis, B. Willke, M. H. Wimmer, W. Winkler, C. C. Wipf, H. Wittel, G. Woan, J. Woehler, J. Worden, J. L. Wright, D. S. Wu, G. Wu, J. Yablon, W. Yam, H. Yamamoto, C. C. Yancey, H. Yu, M. Yvert, A. ZadroŻny, L. Zangrando, M. Zanolin, J. P. Zendri, M. Zevin, L. Zhang, M. Zhang, Y. Zhang, C. Zhao, M. Zhou, Z. Zhou, X. J. Zhu, M. E. Zucker, S. E. Zuraw, J. Zweizig, LIGO Scientific Collaboration, and Virgo Collaboration. Binary Black Hole Mergers in the First Advanced LIGO Observing Run. *Physical Review X*, 6(4):041015, October 2016. doi: 10.1103/PhysRevX.6.041015. 1

Pau Amaro-Seoane, Heather Audley, Stanislav Babak, John Baker, Enrico Barausse, Peter Bender, Emanuele Berti, Pierre Binetruy, Michael Born, Daniele Bortoluzzi, Jordan Camp, Chiara Caprini, Vitor Cardoso, Monica Colpi, John Conklin, Neil Cornish, Curt Cutler, Karsten Danzmann, Rita Dolesi, Luigi Ferraioli, Valerio Ferroni, Ewan Fitzsimons, Jonathan Gair, Lluis Gesa Bote, Domenico Giardini, Ferran Gibert, Catia Grimani, Hubert Halloin, Gerhard Heinzel, Thomas Hertog, Martin Hewitson, Kelly Holley-Bockelmann, Daniel Hollington, Mauro Hueller, Henri Inchauspe, Philippe Jetzer, Nikos Karnesis, Christian Killow, Antoine Klein, Bill Klipstein, Natalia Korsakova, Shane L Lar-

son, Jeffrey Livas, Ivan Lloro, Nary Man, Davor Mance, Joseph Martino, Ignacio Mateos, Kirk McKenzie, Sean T McWilliams, Cole Miller, Guido Mueller, Germano Nardini, Gijs Nelemans, Miquel Nofrarias, Antoine Petiteau, Paolo Pivato, Eric Plagnol, Ed Porter, Jens Reiche, David Robertson, Norna Robertson, Elena Rossi, Giuliana Russano, Bernard Schutz, Alberto Sesana, David Shoemaker, Jacob Slutsky, Carlos F. Sopuerta, Tim Sumner, Nicola Tamanini, Ira Thorpe, Michael Troebs, Michele Vallisneri, Alberto Vecchio, Daniele Vetrugno, Stefano Vitale, Marta Volonteri, Gudrun Wanner, Harry Ward, Peter Wass, William Weber, John Ziemer, and Peter Zweifel. Laser Interferometer Space Antenna. *arXiv e-prints*, art. arXiv:1702.00786, February 2017. 1

Andrea N Lommen. Pulsar timing arrays: the promise of gravitational wave detection. *Reports on Progress in Physics*, 78(12):124901, 2015. 1

Xavier Siemens, Justin Ellis, Fredrick Jenet, and Joseph D. Romano. The stochastic background: scaling laws and time to detection for pulsar timing arrays. *Classical and Quantum Gravity*, 30(22):224015, November 2013. doi: 10.1088/0264-9381/30/22/224015. 1

B. B. P. Perera, M. E. DeCesar, P. B. Demorest, M. Kerr, L. Lentati, D. J. Nice, S. Osłowski, S. M. Ransom, M. J. Keith, Z. Arzoumanian, M. Bailes, P. T. Baker, C. G. Bassa, N. D. R. Bhat, A. Brazier, M. Burgay, S. Burke-Spolaor, R. N. Caballero, D. J. Champion, S. Chatterjee, S. Chen, I. Cognard, J. M. Cordes, K. Crowter, S. Dai, G. Desvignes, T. Dolch, R. D. Ferdman, E. C. Ferrara, E. Fonseca, J. M. Goldstein, E. Graikou, L. Guillemot, J. S. Hazboun, G. Hobbs, H. Hu, K. Islo, G. H. Janssen, R. Karuppusamy, M. Kramer, M. T. Lam, K. J. Lee, K. Liu, J. Luo, A. G. Lyne, R. N. Manchester, J. W. McKee, M. A. McLaughlin, C. M. F. Mingarelli, A. P. Parthasarathy, T. T. Pennucci, D. Perrodin, A. Possenti, D. J. Reardon, C. J. Russell, S. A. Sanidas, A. Sesana, G. Shaifullah, R. M. Shannon, X. Siemens, J. Simon, R. Spiewak, I. H. Stairs, B. W. Stappers, J. K. Swiggum, S. R. Taylor, G. Theureau, C. Tiburzi, M. Vallisneri, A. Vecchio, J. B. Wang, S. B. Zhang, L. Zhang, W. W. Zhu, and X. J. Zhu. The International Pulsar Timing Array: second data release. , 490(4):4666–4687, December 2019. doi: 10.1093/mnras/stz2857. 1

Z. Arzoumanian, A. Brazier, S. Burke-Spolaor, S. J. Chamberlin, S. Chatterjee, B. Christy,

J. M. Cordes, N. J. Cornish, K. Crowter, P. B. Demorest, X. Deng, T. Dolch, J. A. Ellis, R. D. Ferdman, E. Fonseca, N. Garver-Daniels, M. E. Gonzalez, F. Jenet, G. Jones, M. L. Jones, V. M. Kaspi, M. Koop, M. T. Lam, T. J. W. Lazio, L. Levin, A. N. Lommen, D. R. Lorimer, J. Luo, R. S. Lynch, D. R. Madison, M. A. McLaughlin, S. T. McWilliams, C. M. F. Mingarelli, D. J. Nice, N. Palliyaguru, T. T. Pennucci, S. M. Ransom, L. Sampson, S. A. Sanidas, A. Sesana, X. Siemens, J. Simon, I. H. Stairs, D. R. Stinebring, K. Stovall, J. Swiggum, S. R. Taylor, M. Vallisneri, R. van Haasteren, Y. Wang, W. W. Zhu, and NANOGrav Collaboration. The NANOGrav Nine-year Data Set: Limits on the Isotropic Stochastic Gravitational Wave Background. , 821(1):13, April 2016. doi: 10.3847/0004-637X/821/1/13. 1, 2

Brian J Burt, Andrea N Lommen, and Lee S Finn. Optimizing pulsar timing arrays to maximize gravitational wave single-source detection: a first cut. *The Astrophysical Journal*, 730(1):17, 2011. 1

Joseph Simon, Abigail Polin, Andrea Lommen, Ben Stappers, Lee Samuel Finn, FA Jenet, and B Christy. Gravitational wave hotspots: ranking potential locations of single-source gravitational wave emission. *The Astrophysical Journal*, 784(1):60, 2014. 1

M Vallisneri, SR Taylor, J Simon, WM Folkner, RS Park, C Cutler, JA Ellis, TJW Lazio, SJ Vigeland, K Aggarwal, et al. Modeling the uncertainties of solar system ephemerides for robust gravitational-wave searches with pulsar-timing arrays. *The Astrophysical Journal*, 893(2):112, 2020. 1

Justin A Ellis, Michele Vallisneri, Stephen R Taylor, and Paul T Baker. Enterprise: Enhanced numerical toolbox enabling a robust pulsar inference suite. *Astrophysics Source Code Library*, pages ascl–1912, 2019. 1

K Aggarwal, Z Arzoumanian, PT Baker, A Brazier, MR Brinson, PR Brook, S Burke-Spolaor, S Chatterjee, JM Cordes, NJ Cornish, et al. The nanograv 11 yr data set: limits on gravitational waves from individual supermassive black hole binaries. *The Astrophysical Journal*, 880(2):116, 2019. 1

K. Aggarwal, Z. Arzoumanian, P. T. Baker, A. Brazier, M. R. Brinson, P. R. Brook, S. Burke-Spolaor, S. Chatterjee, J. M. Cordes, N. J. Cornish, F. Crawford, K. Crowter, H. T. Cromartie, M. DeCesar, P. B. Demorest, T. Dolch, J. A. Ellis, R. D. Ferdman, E. Ferrara, E. Fonseca, N. Garver-Daniels, P. Gentile, J. S. Hazboun, A. M. Holgado, E. A. Huerta, K. Islo, R. Jennings, G. Jones, M. L. Jones, A. R. Kaiser, D. L. Kaplan, L. Z. Kelley, J. S. Key, M. T. Lam, T. J. W. Lazio, L. Levin, D. R. Lorimer, J. Luo, R. S. Lynch, D. R. Madison, M. A. McLaughlin, S. T. McWilliams, C. M. F. Mingarelli, C. Ng, D. J. Nice, T. T. Pennucci, N. S. Pol, S. M. Ransom, P. S. Ray, X. Siemens, J. Simon, R. Spiewak, I. H. Stairs, D. R. Stinebring, K. Stovall, J. Swiggum, S. R. Taylor, J. E. Turner, M. Vallisneri, R. van Haasteren, S. J. Vigeland, C. A. Witt, W. W. Zhu, and NANOGrav Collaboration. The NANOGrav 11 yr Data Set: Limits on Gravitational Waves from Individual Supermassive Black Hole Binaries. , 880(2):116, August 2019. doi: 10.3847/1538-4357/ab2236. 1

Zaven Arzoumanian, Paul T. Baker, Harsha Blumer, Bence Bécsy, Adam Brazier, Paul R. Brook, Sarah Burke-Spolaor, Shami Chatterjee, Siyuan Chen, James M. Cordes, Neil J. Cornish, Fronefield Crawford, H. Thankful Cromartie, Megan E. Decesar, Paul B. Demorest, Timothy Dolch, Justin A. Ellis, Elizabeth C. Ferrara, William Fiore, Emmanuel Fonseca, Nathan Garver-Daniels, Peter A. Gentile, Deborah C. Good, Jeffrey S. Hazboun, A. Miguel Holgado, Kristina Islo, Ross J. Jennings, Megan L. Jones, Andrew R. Kaiser, David L. Kaplan, Luke Zoltan Kelley, Joey Shapiro Key, Nima Laal, Michael T. Lam, T. Joseph W. Lazio, Duncan R. Lorimer, Jing Luo, Ryan S. Lynch, Dustin R. Madison, Maura A. McLaughlin, Chiara M. F. Mingarelli, Cherry Ng, David J. Nice, Timothy T. Pennucci, Nihan S. Pol, Scott M. Ransom, Paul S. Ray, Brent J. Shapiro-Albert, Xavier Siemens, Joseph Simon, Renée Spiewak, Ingrid H. Stairs, Daniel R. Stinebring, Kevin Stovall, Jerry P. Sun, Joseph K. Swiggum, Stephen R. Taylor, Jacob E. Turner, Michele Vallisneri, Sarah J. Vigeland, Caitlin A. Witt, and Nanograv Collaboration. The NANOGrav 12.5 yr Data Set: Search for an Isotropic Stochastic Gravitational-wave Background. , 905(2):L34, December 2020. doi: 10.3847/2041-8213/abd401. 1, 2

G. Desvignes, R. N. Caballero, L. Lentati, J. P. W. Verbiest, D. J. Champion, B. W. Stappers,

G. H. Janssen, P. Lazarus, S. Osłowski, S. Babak, C. G. Bassa, P. Brem, M. Burgay, I. Cognard, J. R. Gair, E. Graikou, L. Guillemot, J. W. T. Hessels, A. Jessner, C. Jordan, R. Karuppusamy, M. Kramer, A. Lassus, K. Lazaridis, K. J. Lee, K. Liu, A. G. Lyne, J. McKee, C. M. F. Mingarelli, D. Perrodin, A. Petiteau, A. Possenti, M. B. Purver, P. A. Rosado, S. Sanidas, A. Sesana, G. Shaifullah, R. Smits, S. R. Taylor, G. Theureau, C. Tiburzi, R. van Haasteren, and A. Vecchio. High-precision timing of 42 millisecond pulsars with the European Pulsar Timing Array. , 458(3):3341–3380, May 2016. doi: 10.1093/mnras/stw483. 1

L. Lentati, S. R. Taylor, C. M. F. Mingarelli, A. Sesana, S. A. Sanidas, A. Vecchio, R. N. Caballero, K. J. Lee, R. van Haasteren, S. Babak, C. G. Bassa, P. Brem, M. Burgay, D. J. Champion, I. Cognard, G. Desvignes, J. R. Gair, L. Guillemot, J. W. T. Hessels, G. H. Janssen, R. Karuppusamy, M. Kramer, A. Lassus, P. Lazarus, K. Liu, S. Osłowski, D. Perrodin, A. Petiteau, A. Possenti, M. B. Purver, P. A. Rosado, R. Smits, B. Stappers, G. Theureau, C. Tiburzi, and J. P. W. Verbiest. European Pulsar Timing Array limits on an isotropic stochastic gravitational-wave background. , 453(3):2576–2598, November 2015. doi: 10.1093/mnras/stv1538. 1

R. N. Manchester, G. Hobbs, M. Bailes, W. A. Coles, W. van Straten, M. J. Keith, R. M. Shannon, N. D. R. Bhat, A. Brown, S. G. Burke-Spolaor, D. J. Champion, A. Chaudhary, R. T. Edwards, G. Hampson, A. W. Hotan, A. Jameson, F. A. Jenet, M. J. Kesteven, J. Khoo, J. Kocz, K. Maciesiak, S. Oslowski, V. Ravi, J. R. Reynolds, J. M. Sarkissian, J. P. W. Verbiest, Z. L. Wen, W. E. Wilson, D. Yardley, W. M. Yan, and X. P. You. The Parkes Pulsar Timing Array Project. , 30:e017, January 2013. doi: 10.1017/pasa.2012.017. 1

D. J. Reardon, G. Hobbs, W. Coles, Y. Levin, M. J. Keith, M. Bailes, N. D. R. Bhat, S. Burke-Spolaor, S. Dai, M. Kerr, P. D. Lasky, R. N. Manchester, S. Osłowski, V. Ravi, R. M. Shannon, W. van Straten, L. Toomey, J. Wang, L. Wen, X. P. You, and X. J. Zhu. Timing analysis for 20 millisecond pulsars in the Parkes Pulsar Timing Array. , 455(2): 1751–1769, January 2016. doi: 10.1093/mnras/stv2395. 1

Ryan M Shannon, Vikram Ravi, WA Coles, George Hobbs, MJ Keith, RN Manchester, J Stuart B Wyithe, M Bailes, NDR Bhat, Sarah Burke-Spolaor, et al. Gravitational-wave limits from pulsar timing constrain supermassive black hole evolution. *Science*, 342(6156): 334–337, 2013. 1

Ryan M Shannon, Vikram Ravi, LT Lentati, Paul Daniel Lasky, G Hobbs, Matthew Kerr, Richard Norman Manchester, William A Coles, Yuri Levin, Matthew Bailes, et al. Gravitational waves from binary supermassive black holes missing in pulsar observations. *Science*, 349(6255):1522–1525, 2015. 1

W. W. Zhu, I. H. Stairs, P. B. Demorest, D. J. Nice, J. A. Ellis, S. M. Ransom, Z. Arzoumanian, K. Crowter, T. Dolch, R. D. Ferdman, E. Fonseca, M. E. Gonzalez, G. Jones, M. L. Jones, M. T. Lam, L. Levin, M. A. McLaughlin, T. Pennucci, K. Stovall, and J. Swiggum. Testing Theories of Gravitation Using 21-Year Timing of Pulsar Binary J1713+0747. , 809(1):41, August 2015. doi: 10.1088/0004-637X/809/1/41. 1

V. M. Kaspi, J. H. Taylor, and M. F. Ryba. High-Precision Timing of Millisecond Pulsars. III. Long-Term Monitoring of PSRs B1855+09 and B1937+21. , 428:713, June 1994. doi: 10.1086/174280. 1

R. M. Shannon, V. Ravi, L. T. Lentati, P. D. Lasky, G. Hobbs, M. Kerr, R. N. Manchester, W. A. Coles, Y. Levin, M. Bailes, N. D. R. Bhat, S. Burke-Spolaor, S. Dai, M. J. Keith, S. Osłowski, D. J. Reardon, W. van Straten, L. Toomey, J. B. Wang, L. Wen, J. S. B. Wyithe, and X. J. Zhu. Gravitational waves from binary supermassive black holes missing in pulsar observations. *Science*, 349(6255):1522–1525, September 2015. doi: 10.1126/science.aab1910. 1

GB Hobbs, RT Edwards, and RN Manchester. Tempo2, a new pulsar-timing package–i. an overview. *Monthly Notices of the Royal Astronomical Society*, 369(2):655–672, 2006. 1

G. Hobbs, F. Jenet, K. J. Lee, J. P. W. Verbiest, D. Yardley, R. Manchester, A. Lommen, W. Coles, R. Edwards, and C. Shettigara. TEMPO2: a new pulsar timing package - III. Gravitational wave simulation. , 394(4):1945–1955, April 2009. doi: 10.1111/j.1365-2966.2009.14391.x. 1

R. T. Edwards, G. B. Hobbs, and R. N. Manchester. TEMPO2, a new pulsar timing package - II. The timing model and precision estimates. , 372(4):1549–1574, November 2006. doi: 10.1111/j.1365-2966.2006.10870.x. 1

S. R. Taylor, L. Lentati, S. Babak, P. Brem, J. R. Gair, A. Sesana, and A. Vecchio. All correlations must die: Assessing the significance of a stochastic gravitational-wave background in pulsar timing arrays. , 95(4):042002, February 2017. doi: 10.1103/PhysRevD.95.042002. 2, 2

Bradley Efron and Robert J Tibshirani. *An introduction to the bootstrap*. CRC press, 1994. 2

SR Taylor, PT Baker, JS Hazboun, JJ Simon, and SJ Vigeland. Enterprise_extensions, 2018. 3

Hazboun J. Ellis J. Pennucci T. Mingarelli C. Simon J. Taylor S. R. Goldstein J. Baker, P. T. Ipta$_d r2_a nalysis.$, 2019. 3